

# Thermoelectric effect in a superconductor with Bogoliubov Fermi surfaces

Tomoya Sano,<sup>1</sup> Takumi Sato,<sup>1,2</sup> Akihiro Sasaki,<sup>1</sup> Satoshi Ikegaya,<sup>3,4</sup> Shingo Kobayashi,<sup>5</sup> and Yasuhiro Asano<sup>1</sup>

<sup>1</sup>*Department of Applied Physics, Hokkaido University, Sapporo 060-8628, Japan*

<sup>2</sup>*Graduate School of Science, Hokkaido University, Sapporo 060-0810, Japan*

<sup>3</sup>*Department of Applied Physics, Nagoya University, Nagoya 464-8603, Japan*

<sup>4</sup>*Institute for Advanced Research, Nagoya University, Nagoya 464-8601, Japan*

<sup>5</sup>*RIKEN Center for Emergent Matter Science, Wako, Saitama 351-0198, Japan*

(Dated: November 12, 2024)

We study theoretically the thermoelectric effect in a superconducting state having the Bogoliubov-Fermi surfaces which stays in a thin superconducting layer between a conventional superconductor and an insulator. The thermoelectric coefficients calculated based on the linear response theory show the remarkable anisotropy in real space, which are explained well by the anisotropic shape of the Bogoliubov-Fermi surface in momentum space. Our results indicate a way to check the existence of the Bogoliubov-Fermi surfaces in a stable superconducting state because the anisotropy is controlled by the direction of an applied magnetic field.

## I. INTRODUCTION

In a superconductor belonging to unconventional symmetry class such as  $d$ -wave and  $p$ -wave, a Bogoliubov quasiparticle at zero energy (Fermi level) exists only at nodes of the pair potential. This conclusion is valid when the superconducting states are described effectively by the  $2 \times 2$  Bogoliubov-de Gennes (BdG) Hamiltonian. When an electron has internal degrees of freedom, such as spin and sublattice, the size of the BdG Hamiltonian becomes as large as  $4 \times 4$  or more. A Bogoliubov quasiparticle in such superconducting states can form Fermi surfaces called Bogoliubov-Fermi surfaces (BFSs) [1–3]. Therefore, multiband superconductors,  $j = 3/2$  superconductors, and usual  $s = 1/2$  superconductors with spin-dependent potentials can have the BFSs in their superconducting states [3–13].

The residual finite density of states (DOS) at zero energy is a direct consequence of the BFSs, which modifies the specific heat and the tunnel spectra [6, 14–17]. Measurements of the specific heat and the magnetic properties at low temperatures has suggested the existence of the BFSs in  $\text{FeSe}_{1-x}\text{S}_x$  [18–23]. However, it is difficult to confirm the existence of the BFSs only by thermodynamic properties because the residual density of states is derived also from random impurities. The instability of the BFSs has been pointed out by a numerical simulation for  $j = 3/2$  superconductors [5, 24]. The instability is partially derived from a fact that quasiparticles on the BFSs coexist with odd-frequency Cooper pairs. [25–27] A possibility of an odd-frequency superconductivity has been discussed as a result of Cooper pairing of two quasiparticles on the BFSs [28]. In order to establish the physics of quasiparticles on the BFSs, it is necessary to clarify phenomena specific to quasiparticles on the BFSs. In what follows, we address these issues.

In this paper, we theoretically discuss the thermoelectric effect due to the quasiparticle on the BFSs. The electric current  $\mathbf{j}$  flows in the presence of the spatial gradient of a temperature  $\nabla T$ . In the relation  $\mathbf{j} = -\alpha \nabla T$ ,

the thermoelectric coefficient  $\alpha$  represents the strength of the effect. The thermoelectric coefficient in a uniform of superconductor  $\alpha_S$  has been formulated in terms of the solutions of the transport equation [29, 30] and the quasiclassical Green's functions [31]. The expression at low temperatures  $\alpha_S \approx \alpha_N \exp(-\Delta/T)$  suggests that the thermoelectric coefficient of a conventional superconductor is exponentially smaller than that in the normal state  $\alpha_N$ . The results can be explained well by the absence of the DOS around zero energy due to the pair potential  $\Delta$ . We discuss the effects of a quasiparticle on the BFSs on the thermoelectric effect in a stable superconducting state at a semiconductor thin film as illustrated in Fig. 1. The BFSs appear at the film in the presence of both spin-orbit interactions (SOI) and strong magnetic fields [7, 32]. The thermoelectric coefficient is calculated based on the linear response theory by using the Keldysh Green's function method. The calculated results show that the thermoelectric effect is anisotropic in real space, which reflects the anisotropic shape of the BFSs in momentum space. Moreover, the thermoelectric coefficient in the presence of the BFSs can be larger than its normal state value. The enhancement in the thermoelectric effect is explained by the shift of the gapped DOS due to a magnetic field. We conclude that the existence of the BFSs can be directly confirmed by the anisotropy of the thermoelectric coefficient.

This paper is organized as follows. In Sec. II, we explain why a complicated junction structure is necessary to observe the thermoelectric effect by focusing on the instability of superconducting states having BFSs. In Sec. III, the calculated results of the DOS and those of the thermoelectric coefficients are presented. We discuss the meaning of the obtained results in Sec. IV. The conclusion is given in Sec. V. The expression of the thermoelectric coefficient is derived based on the linear response theory in Appendix A.

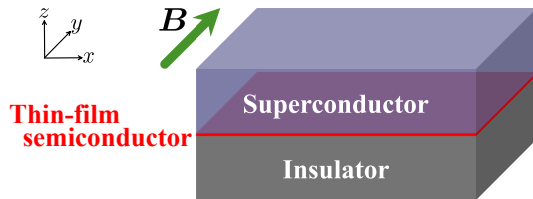


FIG. 1. Schematics of a proximity structure considered in this paper. We focus on two-dimensional electronic states at a thin semiconductor sandwiched between a superconductor and an insulator. Because of inversion symmetry breaking in the  $z$  direction, Rashba spin-orbit interaction works for electrons. In the presence of an external magnetic field applied in the  $y$  direction and the proximity-effect induced pair potential, a superconducting state with Bogoliubov-Fermi surfaces can be realized in the thin film.

## II. MODEL

We discuss the thermoelectric effect in two-dimensional electronic states realized in a thin semiconductor sandwiched by a spin-singlet  $s$ -wave superconductor and an insulator under an in-plane magnetic field as illustrated in Fig. 1. The BdG Hamiltonian reads

$$\check{H}_{\text{BdG}} = \begin{bmatrix} \hat{h}_N(\mathbf{k}) & \Delta i\hat{\sigma}_y \\ -\Delta i\hat{\sigma}_y & -\hat{h}_N^*(-\mathbf{k}) \end{bmatrix}, \quad (1)$$

$$\hat{h}_N(\mathbf{k}) = \xi_{\mathbf{k}}\hat{\sigma}_0 - \mathbf{V} \cdot \hat{\boldsymbol{\sigma}} - \boldsymbol{\lambda} \times \mathbf{k} \cdot \hat{\boldsymbol{\sigma}}, \quad (2)$$

$$\xi_{\mathbf{k}} = \hbar^2 \mathbf{k}^2 / (2m) - \mu, \quad \mathbf{V} = (0, V, 0), \quad (3)$$

with  $V = \frac{1}{2}g\mu_B B$ , where  $\mu$  is the chemical potential,  $B$  is the amplitude of an external magnetic field in the  $y$  direction,  $g$  is the  $g$ -factor, and  $\mu_B$  is the Bohr magneton. Due to the absence of inversion symmetry in the  $z$  direction, the Rashba SOI works for electrons with  $\boldsymbol{\lambda} = (0, 0, \lambda)$ . The Pauli's matrices in spin space are denoted by  $\hat{\boldsymbol{\sigma}} = (\hat{\sigma}_x, \hat{\sigma}_y, \hat{\sigma}_z)$  and  $\hat{\sigma}_0$  is the unit matrix in spin space. The pair potential at the thin film is  $\Delta$ . The reasons why we need to consider such a junction are explained below.

It is widely accepted that spin-singlet superconductivity is fragile in strong Zeeman potential  $V$ . However, to realize the BFSs in a conventional superconductor [7, 32], the amplitude of a Zeeman field must be larger than the Clogston-Chandrasekhar limit [33, 34]. Here, we assume that the pair potential  $\Delta$  is induced in a thin semiconductor due to the proximity effect from a parent superconductor. In such a system, induced pair potential would be smaller than that of the parent superconductor  $\Delta_{\text{bulk}}$ . In addition, it would be possible to choose a semiconductor with a large  $g$ -factor ( $g > 2$ ) [35–39], which enables a larger Zeeman potential in a semiconductor  $V$  than that in the bulk of superconductor  $V_{\text{bulk}}$ . For example,  $g \sim 10$  or larger was reported in a two dimensional Al-InAs hybrid system [35–38]. A condition for the appearance of

the BFSs in a thin semiconductor

$$\Delta < V = \frac{1}{2}g\mu_B B, \quad (4)$$

and that for the stable superconducting state in the bulk

$$\Delta_{\text{bulk}} \gg V_{\text{bulk}} \sim \mu_B B, \quad (5)$$

can be satisfied simultaneously in the proximity structure in Fig. 1. In what follows, we also assume that the transition to superconducting phase is always the second-order [27] and that the dependence of  $\Delta$  on temperatures is described by BCS theory.

In a junction shown in Fig. 1, the thermoelectric current flows only in the semiconducting segment. The electric current is absent in an insulator. Furthermore, the thermoelectric coefficient in the parent superconductor is almost zero at low temperatures [30],

$$\alpha_S \approx \alpha_N \exp(-\Delta_{\text{bulk}}/T) \ll \alpha_N, \quad (6)$$

$$\alpha_N = \frac{\pi^2}{6d\delta} e\hbar T C_0, \quad C_0 = \frac{d}{d\xi} N(\xi) v^2(\xi) \Big|_{\xi=0}, \quad (7)$$

where  $\delta \ll 1$  is a positive small real number,  $N$  is the DOS per volume in the normal state, and  $\mathbf{v} = \hbar\mathbf{k}/m$  is the group velocity. Therefore, the electric current flowing through the semiconducting film dominates the thermoelectric effect of whole structure in Fig. 1.

The thermoelectric coefficient is calculated based on the linear response theory. Details of the derivation are given in Appendix A. The electric currents is represented by the Keldysh-Green's function as shown in Eq. (A8). The thermal gradient is considered through the distribution function in Eq. (A25). Within the first order of  $\nabla T$ , the diagonal element of the thermoelectric coefficient is calculated as

$$\alpha^\nu = \frac{e\hbar}{32\pi T^2} \int_{-\infty}^{\infty} d\epsilon \frac{\epsilon}{\cosh^2(\epsilon/2T)} \times \int \frac{d\hat{\mathbf{k}}}{2\pi} \left( \hat{k}^\nu \right)^2 \int_{-\infty}^{\infty} d\xi N(\xi) v^2(\xi) I(\mathbf{k}, \epsilon), \quad (8)$$

$$I(\mathbf{k}, \epsilon) = \text{Tr} \left[ \hat{G}(\hat{G} - \hat{G}^\dagger) - \hat{Q}(\hat{Q} - \hat{Q}^\dagger) + \hat{F}\hat{F}^\dagger - \hat{F}\hat{F}^\dagger \right]_{(\mathbf{k}, \epsilon)}^R, \quad (9)$$

with  $\nu = x$  or  $y$ , where  $T$  is a temperature in equilibrium and  $R$  in the superscript of Eq. (9) means that all the Green's functions belong to the retarded causality. We have used a relation

$$\frac{1}{V_{\text{vol}}} \sum_{\mathbf{k}} \rightarrow \int \frac{d\hat{\mathbf{k}}}{2\pi} \int_{-\infty}^{\infty} d\xi N(\xi), \quad (10)$$

with  $\hat{\mathbf{k}} = (k_x, k_y)/|\mathbf{k}|$ . The  $2 \times 2$  retarded Green's functions in Eq. (9) are the solution of the Gor'kov equation,

$$[\epsilon + i\delta - \check{H}_{\text{BdG}}] \begin{bmatrix} \hat{G} & \hat{F} \\ -\hat{F} & -\hat{Q} \end{bmatrix}_{(\mathbf{k}, \epsilon)}^R = \check{1}. \quad (11)$$

For numerical simulation, we put  $\delta = 10^{-4}\Delta_0$  and  $\Delta_0 = 0.02\mu$ , where  $\Delta_0$  is the amplitude of induced pair potential at zero temperature. The Green's functions are calculated to be

$$\hat{G}(\mathbf{k}, \epsilon) = \frac{1}{Z} [(\epsilon - \xi_{\mathbf{k}}) \hat{z}_N - (\epsilon + \xi_{\mathbf{k}}) \Delta^2 - \mathbf{V} \cdot \hat{\sigma}(\hat{z}_N + \Delta^2) - \boldsymbol{\alpha}_{\mathbf{k}} \cdot \hat{\sigma}(\hat{z}_N - \Delta^2)], \quad (12)$$

$$\hat{F}(\mathbf{k}, \epsilon) = \frac{1}{Z} [(\epsilon^2 - \xi_{\mathbf{k}}^2 - \Delta^2 - \boldsymbol{\alpha}_{\mathbf{k}}^2 + \mathbf{V}^2) - 2\epsilon \mathbf{V} \cdot \hat{\sigma} - 2\xi_{\mathbf{k}} \boldsymbol{\alpha}_{\mathbf{k}} \cdot \hat{\sigma} - 2i\mathbf{V} \times \boldsymbol{\alpha}_{\mathbf{k}} \cdot \hat{\sigma}] \Delta i \hat{\sigma}_y, \quad (13)$$

$$Z = (\epsilon^2 - \xi_{\mathbf{k}}^2 - \Delta^2 - \boldsymbol{\alpha}_{\mathbf{k}}^2 + \mathbf{V}^2)^2 + 4(\mathbf{V} \times \boldsymbol{\alpha}_{\mathbf{k}})^2 - 4(\epsilon \mathbf{V} + \xi_{\mathbf{k}} \boldsymbol{\alpha}_{\mathbf{k}})^2, \quad (14)$$

$$\hat{z}_N = (\epsilon + \xi_{\mathbf{k}})^2 - (\mathbf{V} - \boldsymbol{\alpha}_{\mathbf{k}})^2, \quad \boldsymbol{\alpha}_{\mathbf{k}} = \boldsymbol{\lambda} \times \mathbf{k}. \quad (15)$$

The density of states per volume are calculated as

$$N(E) = \int \frac{d\hat{\mathbf{k}}}{2\pi} n(\hat{\mathbf{k}}, E), \quad (16)$$

$$n(\hat{\mathbf{k}}, E) = \frac{-N_0}{8\pi i} \int_{-\infty}^{\infty} d\xi \text{Tr} \left[ \hat{G} - \hat{G}^\dagger - \hat{G} + \hat{G}^\dagger \right]_{(\mathbf{k}, E)}^R, \quad (17)$$

where  $n(\hat{\mathbf{k}}, E)$  is the angle-resolved density of states and  $N_0$  is the DOS per volume in the normal states at the Fermi level.

### III. RESULTS

#### A. Density of states

In Fig. 2, we plot the BFSs (possible wavenumber for zero-energy eigenvalue) for several choices of Zeeman potentials  $V = \frac{1}{2}g\mu_B B$ . For Zeeman potentials slightly larger than  $\Delta_0$  in Figs. 2(a) and (b), the quasiparticle states at zero energy appear around  $\mathbf{k} = (k_x, k_y) = (\pm k_F, 0)$ . The size of the BFSs increases with the increase of  $V$  as shown in Figs. 2(c) and (d). The results show that the quasiparticle states are absent around  $\mathbf{k} = (0, \pm k_F)$ . The original Fermi surface in the normal state, given approximately by  $k_x^2 + k_y^2 = k_F^2$ , has a circular shape and is isotropic in momentum space. However, the BFSs in Figs. 2 is anisotropic in momentum space, which is a source of the anisotropy in the thermoelectric effect. In Fig. 2, the strength of the Rashba SOI is fixed at  $\lambda k_F = 2\Delta_0$ . Changing the amplitude of  $\lambda$  shifts the place of the BFSs only slightly in momentum space. We choose  $\lambda k_F = 2\Delta_0$  throughout this paper because the characteristic features of the BFSs shown in Fig. 2 are insensitive to the choice of  $\lambda$ .

In Fig. 3, we present the DOS in the presence of the BFSs for several Zeeman potentials. The DOS at zero energy remains a finite value for all the Zeeman potentials. At  $V = 0$ , the DOS has two coherence peaks at  $E = \pm\Delta$ . Zeeman potentials shift these peaks depending on spin of an electron, which explains a peak around

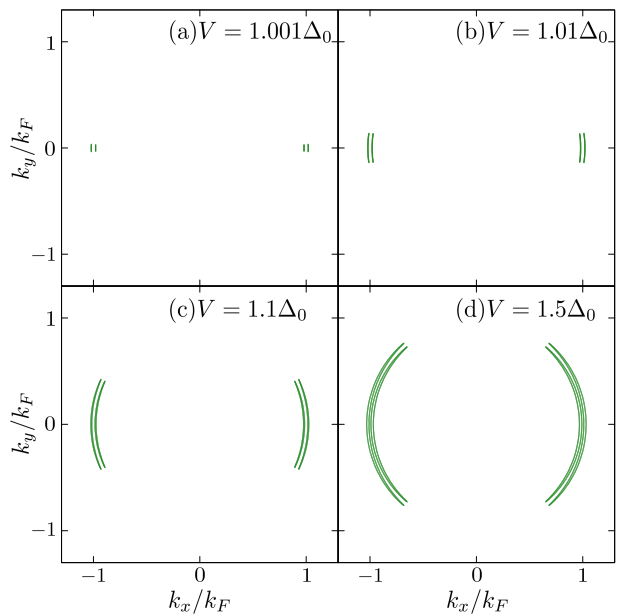


FIG. 2. The BFSs for  $V = 1.001\Delta_0$ ,  $V = 1.01\Delta_0$ ,  $V = 1.1\Delta_0$ , and  $V = 1.5\Delta_0$  are displayed in (a), (b), (c), and (d), respectively. The strength of the Rashba SOI is fixed at  $\lambda k_F = 2\Delta_0$ .

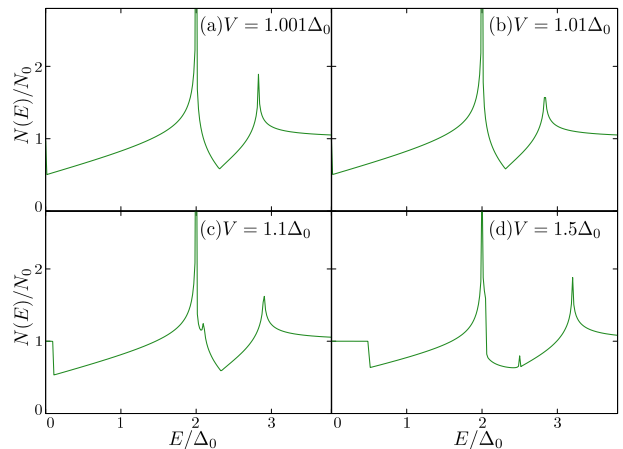


FIG. 3. Density of states calculated for several Zeeman potentials at  $\lambda k_F = 2\Delta_0$ .

$E/\Delta_0 = 2$  in Fig. 3. As Zeeman potentials increase, the width of a plateau near zero energy increases. This makes a superconducting phase with the BFSs unstable thermodynamically. To gain the condensation energy, the gapped energy spectra in DOS are necessary. The BFSs in the two-dimensional superconducting states is stabilized by the superconducting condensate in the parent superconductor.

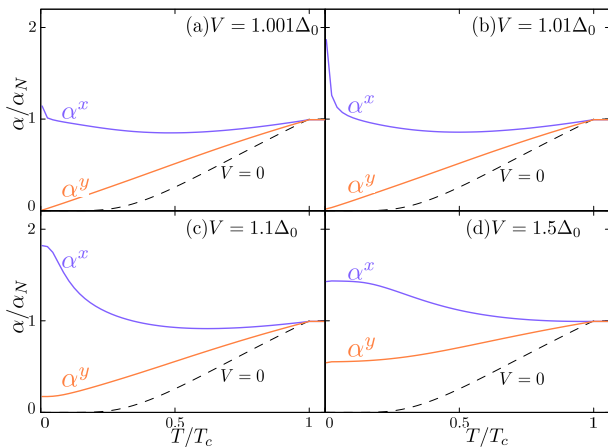


FIG. 4. The thermoelectric coefficient versus temperature. The coefficients in the two directions are shown with  $\alpha^x$  and  $\alpha^y$ . The broken lines show the results in the absence of a Zeeman potential.

### B. Thermoelectric effect

The calculated results of the thermoelectric coefficients in the presence of the BFSs are plotted as a function of temperature for several of Zeeman potentials in Fig 4, where the dependence of  $\Delta$  on temperatures is described by BCS theory. The vertical axis is normalized to the coefficient in the normal state  $\alpha_N$  which is isotropic in real space. The results in the absence of a Zeeman potential are shown with a broken line for comparison and obey  $\alpha \approx \alpha_N \exp(-\Delta/T)$  at low temperatures. Solid lines represent  $\alpha^{x(y)}$  in which the electric current is perpendicular to magnetic field  $\mathbf{j} \perp \mathbf{B}$  (parallel to magnetic field  $\mathbf{j} \parallel \mathbf{B}$ ). The thermoelectric coefficients indicate two characteristic features: the remarkable anisotropy in real space and  $\alpha^x > \alpha_N$ . The anisotropy in the thermoelectric effect originates from the anisotropy of the BFSs in momentum space shown in Fig. 2. The zero-energy states around  $\mathbf{k} = (\pm k_F, 0)$  in Fig. 2 can carry the electric current in the  $x$  direction. However, zero-energy states are absent around  $\mathbf{k} = (0, \pm k_F)$ , which results in the monotonic decrease of  $\alpha^y$  with decreasing temperatures in Fig 4.

To understand the unusual dependence of  $\alpha^x$  on temperature, we analyze the angle-resolved DOS displayed in Fig. 5, where  $n(\hat{\mathbf{k}}, E)$  along the  $k_x$  axis is shown by fixing  $k_y$  at 0. The angle-resolved DOS has two peaks for  $E > 0$  because a Zeeman potential shifts the coherence peaks depending on spins of a quasiparticle. For  $V \approx \Delta$  in Figs. 5(a) and (b), a peak appears almost zero energy in the angle-resolved DOS. A quasiparticle at such zero-energy states carries the thermoelectric current in the  $x$  direction. The relation  $\alpha^x > \alpha_N$  is a result of the shift of the coherence peak by a Zeeman potential. The DOS along the  $k_y$  axis calculated with putting  $k_x = 0$  is shown in Fig. 6. In contrast to Fig. 5, the angle resolved DOS always has the gapped energy spectra at zero energy as a

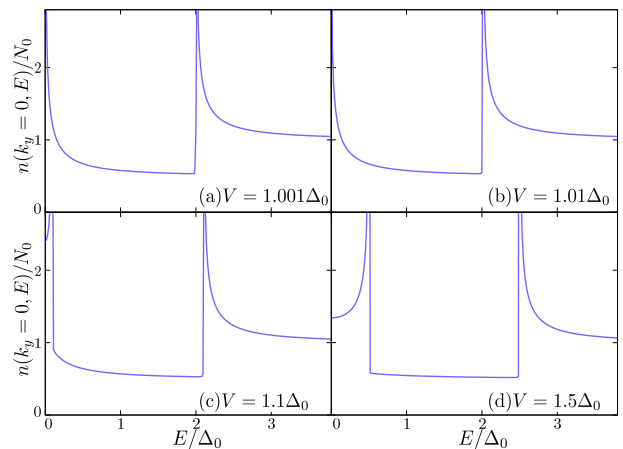


FIG. 5. The angle-resolved density of states  $n(\hat{\mathbf{k}}, E)$  at  $k_y = 0$  are shown for several Zeeman fields with  $\lambda k_F = 2\Delta_0$ .

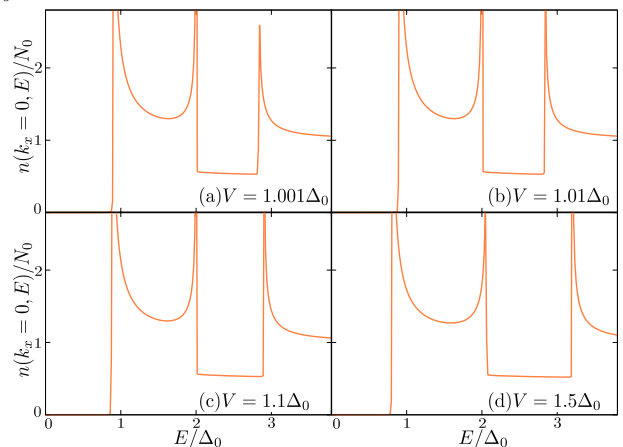


FIG. 6. The angle-resolved density of states  $n(\hat{\mathbf{k}}, E)$  at  $k_x = 0$  are shown for several Zeeman fields with  $\lambda k_F = 2\Delta_0$ .

result of the absence of the BFSs around  $\mathbf{k} = (0, \pm k_F)$  in Fig. 2. This also explains the monotonic dependence of  $\alpha^y$  on temperatures in Fig. 4. The BFSs spreads in the  $k_y$  direction with increasing Zeeman potentials in Fig. 2. As a result,  $\alpha^y$  takes a finite value even at zero temperature. The quasiparticle states with a velocity component in the  $y$  direction increase with increasing Zeeman potentials. We conclude that the thermoelectric effect in a junction in Fig. 1 is remarkably anisotropic in real space because of the anisotropy of the BFSs in momentum space. The thermoelectric coefficient for the current perpendicular to a magnetic field can be larger than that in the normal state because a Zeeman potential shifts the gapped spectra in DOS depending on spin of a quasiparticle.

## IV. DISCUSSION

Two of authors have shown that odd-frequency Cooper pairs coexist with quasiparticles on the BFSs [25]. This can be seen in the expression of the anomalous Green's

function in Eq. (13). The first term represents a spin-singlet Cooper pairs and is linked to the pair potential through the gap equation. The other terms represent spin-triplet Cooper pairs generated by a Zeeman potential and/or the SOI. To make discussion simpler, we put  $\mathbf{V} = \boldsymbol{\alpha}_{\mathbf{k}} = 0$  at the denominator of the Green function in Eq. (14). By applying the analytic continuation  $\epsilon + i\delta \rightarrow i\omega_n$  in such a situation, the second term in Eq. (13) is relating to odd-frequency Cooper pairs because it is an odd function of the Matsubara frequency  $\omega_n$ . Before calculating the thermoelectric coefficients, we had expected the contributions of odd-frequency Cooper pairs to the electric current. Therefore, we formulate the thermoelectric coefficients in terms of the Green's functions of the Gor'kov equation. In fact, the expression in Eq. (9) includes the anomalous Green's function  $\hat{F}$  and  $\hat{F}^\dagger$ . Unfortunately, however, we find that  $\text{Tr}[\hat{F}\hat{F}^\dagger - \hat{F}^\dagger\hat{F}] = 0$  for any Zeeman fields and SOIs in a spin-singlet  $s$ -wave superconductor. Only the normal Green's functions  $\hat{G}$  and  $\hat{G}^\dagger$  contribute to the thermoelectric coefficient in our model. As a result, the characteristic behavior of the thermoelectric coefficients can be explained well by the residual DOS due to quasiparticles on the BFSs.

## V. CONCLUSION

We have studied the thermoelectric effect in a thin superconducting film between a conventional superconductor and an insulator. In the presence of an external magnetic field and the Rashba spin-orbit interactions, the superconducting phase having the Bogoliubov-Fermi surfaces can be realized at the thin film. The thermoelectric coefficient is calculated based on the linear response theory in the presence of the spatial gradient of a temperature. The calculated results of the thermoelectric coefficients show the remarkable anisotropy at low temperatures: the coefficient for the current perpendicular to a magnetic field is larger than that for the current parallel to a magnetic field. Moreover, the coefficient for the current perpendicular to a magnetic field can be larger than its normal state value. These characteristic features of thermoelectric effect are explained well by the anisotropy of the Bogoliubov-Fermi surfaces in momentum space. Our results indicate a way of realizing the stable Bogoliubov-Fermi surfaces and how to check the existence of the Bogoliubov-Fermi surfaces.

## ACKNOWLEDGMENTS

The authors are grateful to Y. Tanaka, Y. Kawaguchi, and S. Hoshino for useful discussions. T. Sato was supported by JST, the establishment of university fellowships towards the creation of science technology innovation, Grant Number JPMJFS2101. S.I. is supported by the Grant-in-Aid for Early-Career Scientists (JSPS

KAKENHI Grant No. JP24K17010). S. K. was supported by JSPS KAKENHI (Grants No. JP19K14612 and No. JP22K03478) and JST CREST (Grant No. JP-MJCR19T2).

## Appendix A: Formalism

### 1. Electric current

To discuss the thermoelectric effect in a bulk of superconductor, we first describe the electric current in terms of Keldysh Green's function,

$$G_{\alpha,\beta}^K(\mathbf{x}_1, \mathbf{x}_2) = -i \times \langle \psi_\alpha(\mathbf{x}_1)\psi_\beta^\dagger(\mathbf{x}_2) - \psi_\beta^\dagger(\mathbf{x}_2)\psi_\alpha(\mathbf{x}_1) \rangle, \quad (\text{A1})$$

$$\underline{G}_{\alpha,\beta}^K(\mathbf{x}_1, \mathbf{x}_2) = -i \times \langle \psi_\alpha^\dagger(\mathbf{x}_1)\psi_\beta(\mathbf{x}_2) - \psi_\beta(\mathbf{x}_2)\psi_\alpha^\dagger(\mathbf{x}_1) \rangle, \quad (\text{A2})$$

where  $\mathbf{x} = (\mathbf{r}, t)$  is the combined representation of coordinate and  $\psi_\alpha(\mathbf{x})$  ( $\psi_\alpha^\dagger(\mathbf{x})$ ) is the annihilation(creation) operator of an electron. By using the anticommutation relations and applying  $\nabla_{\mathbf{r}_1}$  from the left, the current density is expressed in terms of the Keldysh Green's function

$$\mathbf{j}(\mathbf{x}_1) = \frac{e\hbar}{4m} \lim_{\mathbf{x}_1 \rightarrow \mathbf{x}_2} \nabla_{\mathbf{r}_1} \text{Tr} [\check{G}^K(\mathbf{x}_1, \mathbf{x}_2)], \quad (\text{A3})$$

where  $-e$  is the charge of an electron,  $\text{Tr}$  is the trace in spin space and particle-hole space

$$\text{Tr} [\check{G}^K(\mathbf{x}_1, \mathbf{x}_2)] = \sum_{\alpha} (G_{\alpha,\alpha}^K + \underline{G}_{\alpha,\alpha}^K). \quad (\text{A4})$$

In what follows, we apply the mixed representation to the Green's function

$$G(\mathbf{x}_1, \mathbf{x}_2) \rightarrow G(\mathbf{X}, \mathbf{x}) = \int \frac{d\mathbf{k}d\epsilon}{(2\pi)^{d+1}} G(\mathbf{R}, \mathbf{k}, \epsilon) e^{i(\mathbf{k}\cdot\mathbf{r} - \epsilon t)}, \quad (\text{A5})$$

$$\mathbf{X} = \frac{\mathbf{x}_1 + \mathbf{x}_2}{2}, \quad \mathbf{x} = \mathbf{x}_1 - \mathbf{x}_2. \quad (\text{A6})$$

The Green's function is independent of center-of-mass-time  $(t_1 + t_2)/2$  because we consider time-independent phenomena in this paper. We also apply the Fourier transformation to the internal degree of freedom  $\mathbf{x}_1 - \mathbf{x}_2$ . Since  $\nabla_{\mathbf{r}_1} = \nabla_{\mathbf{R}}/2 + \nabla_{\mathbf{r}}$ , we obtain

$$\begin{aligned} & \nabla_{\mathbf{r}_1} G(\mathbf{x}_1, \mathbf{x}_2) \\ &= \int \frac{d\mathbf{k}d\epsilon}{(2\pi)^{d+1}} \left[ \frac{1}{2} \nabla_{\mathbf{R}} + i\mathbf{k} \right] G(\mathbf{R}, \mathbf{k}, \epsilon) e^{i(\mathbf{k}\cdot\mathbf{r} - \epsilon t)}. \end{aligned} \quad (\text{A7})$$

In the mean-field theory of superconductivity, the spatial gradient of the Green's function is estimated as  $|\nabla_{\mathbf{R}} G(\mathbf{R}, \mathbf{k}, \epsilon)| \simeq G(\mathbf{R}, \mathbf{k}, \epsilon)/\xi_0$ , whereas the dominant wavenumber to the integral is  $|\mathbf{k}| \simeq k_F \simeq 1/\lambda_F$ . The coherence length  $\xi_0 = \hbar v_F / (\pi \Delta_0) \simeq \epsilon_F / (\pi k_F T_c)$  is much

longer than the Fermi wavelength  $\lambda_F$ . The first term is negligible because the transition temperature  $T_c$  is much smaller than the Fermi energy  $\epsilon_F$ . The current density is represented as

$$\mathbf{j}(\mathbf{R}) = \frac{e}{4} \int \frac{d\mathbf{k}d\epsilon}{(2\pi)^{d+1}} i\mathbf{v}\text{Tr} [\check{G}^K(\mathbf{R}, \mathbf{k}, \epsilon)]. \quad (\text{A8})$$

## 2. Gor'kov equation

The superconducting state in equilibrium is described by the solution of the Gor'kov equation,

$$\int d\mathbf{x}_2 \begin{bmatrix} \check{L} - \check{\Sigma}^R & -\check{\Sigma}^K \\ 0 & \check{L} - \check{\Sigma}^A \end{bmatrix}_{(\mathbf{x}_1, \mathbf{x}_2)} \begin{bmatrix} \check{G}^R & \check{G}^K \\ 0 & \check{G}^A \end{bmatrix}_{(\mathbf{x}_2, \mathbf{x}_3)} = \begin{bmatrix} \check{1} & 0 \\ 0 & \check{1} \end{bmatrix} \delta(\mathbf{x}_1 - \mathbf{x}_3), \quad (\text{A9})$$

$$\check{L}(\mathbf{x}_1, \mathbf{x}_2) = i\delta(\mathbf{r}_1 - \mathbf{r}_2)\partial_{t_2} - \delta(t_1 - t_2) \left\{ -\frac{\hbar^2}{2m}\nabla_{\mathbf{r}_2}^2 - \mu \right\} \check{\tau}_3 - \check{V}(\mathbf{x}_1, \mathbf{x}_2), \quad (\text{A10})$$

$$\check{V}(\mathbf{x}_1, \mathbf{x}_2) = \delta(\mathbf{x}_1 - \mathbf{x}_2) \begin{bmatrix} \mathbf{V} \cdot \hat{\boldsymbol{\sigma}} - i\boldsymbol{\lambda} \times \hat{\nabla}_{\mathbf{r}_2} \cdot \hat{\boldsymbol{\sigma}} & 0 \\ 0 & -\mathbf{V} \cdot \hat{\boldsymbol{\sigma}}^* - i\boldsymbol{\lambda} \times \hat{\nabla}_{\mathbf{r}_2} \cdot \hat{\boldsymbol{\sigma}}^* \end{bmatrix}, \quad (\text{A11})$$

where  $\check{\tau}_i (i = 1, 2, 3)$  are Pauli's matrix in particle-hole space. The self-energy consists of two contributions,

$$\check{\Sigma}^X(\mathbf{x}_1, \mathbf{x}_2) = \check{\Delta}(\mathbf{x}_1, \mathbf{x}_2) + \check{\Sigma}_{\text{imp}}^X(\mathbf{r}_1 - \mathbf{r}_2)\delta(t_1 - t_2), \quad (X = R, A, K). \quad (\text{A12})$$

The pair potential

$$\check{\Delta}(\mathbf{x}_1, \mathbf{x}_2) = \begin{bmatrix} 0 & \hat{\Delta}(\mathbf{x}_1 - \mathbf{x}_2) \\ -\hat{\Delta}^*(\mathbf{x}_1 - \mathbf{x}_2) & 0 \end{bmatrix}, \quad (\text{A13})$$

is the self-energy due to the attractive interactions. The impurity self-energy is uniform in real space due to ensemble averaging and instantaneous in time. The Green's function is represented by

$$\check{G}(\mathbf{x}_2, \mathbf{x}_3) = \check{G}(\mathbf{R}_{23}, \mathbf{r}_{23}, T_{23}, t_{23}) = \int \frac{d\mathbf{k}d\epsilon}{(2\pi)^{d+1}} \check{G}(\mathbf{R}_{23}, \mathbf{k}, T_{23}, \epsilon) e^{i(\mathbf{k} \cdot \mathbf{r}_{23} - \epsilon t_{23})}, \quad (\text{A14})$$

with

$$\mathbf{R}_{23} = \frac{\mathbf{r}_2 + \mathbf{r}_3}{2}, \quad \mathbf{r}_{23} = \mathbf{r}_2 - \mathbf{r}_3, \quad T_{23} = \frac{t_2 + t_3}{2}, \quad t_{23} = t_2 - t_3. \quad (\text{A15})$$

The derivative in  $\check{L}$  is carried out as

$$\nabla_{\mathbf{r}_2} \check{G}(\mathbf{x}_2, \mathbf{x}_3) = \int \frac{d\mathbf{k}d\epsilon}{(2\pi)^{d+1}} \left\{ \frac{1}{2} \nabla_{\mathbf{R}_{23}} + \nabla_{\mathbf{r}_{23}} \right\} \check{G}(\mathbf{R}_{23}, \mathbf{k}, T_{23}, \epsilon) e^{i(\mathbf{k} \cdot \mathbf{r}_{23} - \epsilon t_{23})}, \quad (\text{A16})$$

$$\simeq \int \frac{d\mathbf{k}d\epsilon}{(2\pi)^{d+1}} i\mathbf{k} \check{G}(\mathbf{R}_{23}, \mathbf{k}, T_{23}, \epsilon) e^{i(\mathbf{k} \cdot \mathbf{r}_{23} - \epsilon t_{23})}, \quad (\text{A17})$$

$$\nabla_{\mathbf{r}_2}^2 \check{G}(\mathbf{x}_2, \mathbf{x}_3) = \int \frac{d\mathbf{k}d\epsilon}{(2\pi)^{d+1}} \left\{ \frac{1}{4} \nabla_{\mathbf{R}_{23}}^2 + \nabla_{\mathbf{R}_{23}} \cdot \nabla_{\mathbf{r}_{23}} + \nabla_{\mathbf{r}_{23}}^2 \right\} \check{G}(\mathbf{R}_{23}, \mathbf{k}, T_{23}, \epsilon) e^{i(\mathbf{k} \cdot \mathbf{r}_{23} - \epsilon t_{23})},$$

$$\simeq \int \frac{d\mathbf{k}d\epsilon}{(2\pi)^{d+1}} \{ i \nabla_{\mathbf{R}_{23}} \cdot \mathbf{k} - \mathbf{k}^2 \} \check{G}(\mathbf{R}_{23}, \mathbf{k}, T_{23}, \epsilon) e^{i(\mathbf{k} \cdot \mathbf{r}_{23} - \epsilon t_{23})}, \quad (\text{A18})$$

$$\begin{aligned} \partial_{t_2} \check{G}(\mathbf{x}_2, \mathbf{x}_3) &= \int \frac{d\mathbf{k}d\epsilon}{(2\pi)^{d+1}} \left\{ \frac{1}{2} \partial_{T_{23}} + \partial_{t_{23}} \right\} \check{G}(\mathbf{R}_{23}, \mathbf{k}, T_{23}, \epsilon) e^{i(\mathbf{k} \cdot \mathbf{r}_{23} - \epsilon t_{23})}, \\ &= \int \frac{d\mathbf{k}d\epsilon}{(2\pi)^{d+1}} i\epsilon \check{G}(\mathbf{R}_{23}, \mathbf{k}, T_{23}, \epsilon) e^{i(\mathbf{k} \cdot \mathbf{r}_{23} - \epsilon t_{23})}. \end{aligned} \quad (\text{A19})$$

We assume that the Green's function is independent of  $T_{ij}$ , because we consider the stationary states. The gradient term  $\nabla_{\mathbf{R}_{23}}G \simeq G/\xi_0$  is much smaller than the remaining term  $\mathbf{k}G \simeq k_F G$  in the weak coupling limit. The Gor'kov equation for a Fourier component is summarized as

$$\left[ \begin{pmatrix} \check{L}_0 + \frac{i}{2}\hbar\mathbf{v} \cdot \nabla_{\mathbf{R}}\check{\tau}_3 & 0 \\ 0 & \check{L}_0 + \frac{i}{2}\hbar\mathbf{v} \cdot \nabla_{\mathbf{R}}\check{\tau}_3 \end{pmatrix} - \begin{pmatrix} \check{\Sigma}^R & \check{\Sigma}^K \\ 0 & \check{\Sigma}^A \end{pmatrix} \right]_{(\mathbf{k}, \epsilon)} \begin{bmatrix} \check{G}^R & \check{G}^K \\ 0 & \check{G}^A \end{bmatrix}_{(\mathbf{R}, \mathbf{k}, \epsilon)} = \begin{bmatrix} \check{1} & 0 \\ 0 & \check{1} \end{bmatrix} \quad (\text{A20})$$

The operators in the Fourier representation are given by

$$\check{L}_0(\mathbf{k}, \epsilon) = \epsilon - \xi_{\mathbf{k}}\check{\tau}_3 - \check{V}, \quad (\text{A21})$$

$$\check{\Sigma}^X = \check{\Delta} - \check{\Sigma}_{\text{imp}}^X, \quad (\text{A22})$$

with

$$\check{\Delta} = \begin{bmatrix} 0 & \hat{\Delta}(\mathbf{k}) \\ -\hat{\Delta}(\mathbf{k}) & 0 \end{bmatrix}, \quad \check{V} = \begin{bmatrix} \mathbf{V} \cdot \hat{\boldsymbol{\sigma}} + \boldsymbol{\lambda} \times \mathbf{k} \cdot \hat{\boldsymbol{\sigma}} & 0 \\ 0 & -\mathbf{V} \cdot \hat{\boldsymbol{\sigma}} + \boldsymbol{\lambda} \times \mathbf{k} \cdot \hat{\boldsymbol{\sigma}} \end{bmatrix}. \quad (\text{A23})$$

The relation

$$\check{Y}(\mathbf{k}, \epsilon) \equiv Y^*(-\mathbf{k}, -\epsilon), \quad (\text{A24})$$

represents particle-hole transformation of a function  $Y(\mathbf{k}, \epsilon)$ .

### 3. Current formula in the linear response

The spatial gradient of temperature is considered through the distribution function

$$\Phi(\epsilon, \mathbf{R}) = \tanh \left[ \frac{\epsilon}{2T(\mathbf{R})} \right]. \quad (\text{A25})$$

The Gor'kov equation becomes

$$\left[ \check{L}_0(\mathbf{k}, \epsilon) - \check{\Sigma}^{R,A}(\mathbf{k}, \epsilon) + \frac{i}{2}\hbar\mathbf{v} \cdot \nabla_{\mathbf{R}}\check{\tau}_3 \right] \left[ \check{G}_0^{R,A}(\mathbf{k}, \epsilon) + \delta\check{G}^{R,A}(\mathbf{R}, \mathbf{k}, \epsilon) \right] = \check{1}, \quad (\text{A26})$$

where  $\delta\check{G}^{R,A}$  is the deviation of the Green's function from their values in equilibrium. Within the first order, we obtain

$$\left[ \check{L}_0(\mathbf{k}, \epsilon) - \check{\Sigma}^{R,A}(\mathbf{k}, \epsilon) \right] \delta\check{G}^{R,A}(\mathbf{R}, \mathbf{k}, \epsilon) = 0, \quad (\text{A27})$$

because  $\nabla_{\mathbf{R}}\check{G}_0^{R,A} = 0$  and Gor'kov equation in equilibrium  $[\check{L}_0(\mathbf{k}, \epsilon) - \check{\Sigma}^{R,A}(\mathbf{k}, \epsilon)]\check{G}_0^{R,A}(\mathbf{k}, \epsilon) = \check{1}$ . The solution is  $\delta\check{G}^{R,A}(\mathbf{R}, \mathbf{k}, \epsilon) = 0$ . The Gor'kov equation for the Keldysh component becomes

$$\left[ \check{L}_0(\mathbf{k}, \epsilon) - \check{\Sigma}^R(\mathbf{k}, \epsilon) + \frac{i}{2}\hbar\mathbf{v} \cdot \nabla_{\mathbf{R}}\check{\tau}_3 \right] \check{G}^K(\mathbf{R}, \mathbf{k}, \epsilon) - \check{\Sigma}^K(\mathbf{k}, \epsilon)\check{G}_0^A(\mathbf{k}, \epsilon) = 0. \quad (\text{A28})$$

We seek the solution of the form

$$\check{G}^K(\mathbf{R}, \mathbf{k}, \epsilon) = \check{G}_0^R(\mathbf{k}, \epsilon)\Phi(\epsilon, \mathbf{R}) - \Phi(\epsilon, \mathbf{R})\check{G}_0^A(\mathbf{k}, \epsilon) + \delta\check{G}^K(\mathbf{R}, \mathbf{k}, \epsilon), \quad (\text{A29})$$

$$\check{\Sigma}^K(\mathbf{k}, \epsilon) = \check{\Sigma}^R(\mathbf{k}, \epsilon)\Phi(\epsilon, \mathbf{R}) - \Phi(\epsilon, \mathbf{R})\check{\Sigma}^A(\mathbf{k}, \epsilon) + \delta\check{\Sigma}^K(\mathbf{R}, \mathbf{k}, \epsilon). \quad (\text{A30})$$

The first term and second term in Eq. (A29) and (A30) are the solutions in equilibrium. We put  $\delta\check{\Sigma}^K = 0$  because the deviation of the self-energy  $\check{\Sigma}$  is considered through the distribution function. We find

$$\delta\check{G}^K = -\frac{i}{2}\hbar\mathbf{v} \cdot \nabla_{\mathbf{R}}\Phi(\epsilon, \mathbf{R}) \left[ \check{G}_0^R(\mathbf{k}, \epsilon)\check{\tau}_3 \{ \check{G}_0^R(\mathbf{k}, \epsilon) - \check{G}_0^A(\mathbf{k}, \epsilon) \} \right]. \quad (\text{A31})$$

By substituting the results into Eq. (A8), the current density is calculated to be

$$\mathbf{j}^\mu(\mathbf{R}) = \frac{e\hbar}{8} \int \frac{d\mathbf{k}d\epsilon}{(2\pi)^{d+1}} \mathbf{v}^\mu \mathbf{v}^\nu \cdot (\nabla_{\mathbf{R}}^\nu \Phi) \text{Tr} \left[ \check{G}_0^R(\mathbf{k}, \epsilon)\check{\tau}_3 \{ \check{G}_0^R(\mathbf{k}, \epsilon) - \check{G}_0^A(\mathbf{k}, \epsilon) \} \right], \quad (\text{A32})$$

$$= -\alpha^{\mu,\nu} \nabla_{\mathbf{R}}^\nu T. \quad (\text{A33})$$

The thermoelectric coefficient is given by

$$\alpha^{\mu,\nu} = \frac{e\hbar}{32\pi T^2} \int_{-\infty}^{\infty} d\epsilon \frac{\epsilon}{\cosh^2(\epsilon/2T)} \int \frac{d\mathbf{k}}{(2\pi)^d} \mathbf{v}^\mu \mathbf{v}^\nu I(\mathbf{k}, \epsilon), \quad (\text{A34})$$

$$= \frac{e\hbar}{32\pi T^2} \int_{-\infty}^{\infty} d\epsilon \frac{\epsilon}{\cosh^2(\epsilon/2T)} \int \frac{d\hat{\mathbf{k}}}{S_d} \hat{k}^\mu \hat{k}^\nu \int_{-\infty}^{\infty} d\xi N(\xi) v^2(\xi) I(\mathbf{k}, \epsilon), \quad (\text{A35})$$

$$I(\mathbf{k}, \epsilon) \equiv \text{Tr} [\check{G}_0^R(\mathbf{k}, \epsilon) \check{\tau}_3 \{ \check{G}_0^R(\mathbf{k}, \epsilon) - \check{G}_0^A(\mathbf{k}, \epsilon) \}], \quad (\text{A36})$$

$$= \text{Tr} \left[ \hat{G}(\hat{G} - \hat{G}^\dagger) - \check{G}(\check{G} - \check{G}^\dagger) + \hat{F}\hat{F}^\dagger - \check{F}\check{F}^\dagger \right]_{(\mathbf{k}, \epsilon)}^R \quad (\text{A37})$$

where  $\mu$  and  $\nu$  are respectively the direction of current density and temperature gradient. Tr in Eq. (A37) means the trace in spin space. The contribution from the anomalous Green's function vanishes by applying Tr for any Zeeman fields and spin-orbit interactions in a spin-singlet s-wave superconductor. We have used the structure of the Green's function in particle-hole space represented as

$$\check{G}^{R,A}(\mathbf{k}, \epsilon) = \begin{bmatrix} \hat{G} & \hat{F} \\ -\check{F} & -\check{G} \end{bmatrix}_{(\mathbf{k}, \epsilon)}, \quad \check{G}^A(\mathbf{k}, \epsilon) = [\check{G}^R(\mathbf{k}, \epsilon)]^\dagger. \quad (\text{A38})$$

The thermoelectric coefficient in a spin-singlet s-wave superconductor is calculated to be

$$\alpha = \alpha_N \frac{3}{2\pi^2} \int_{\Delta/T}^{\infty} dx \frac{x^2}{\cosh^2(x/2)}, \quad (\text{A39})$$

$$\alpha_N = \frac{\pi^2}{3d} e\hbar T \tau C_0, \quad C_0 = \left. \frac{d}{d\xi} N(\xi) v^2(\xi) \right|_{\xi=0}, \quad (\text{A40})$$

where  $\tau$  is the relaxation time due to impurities. The results are identical to the previous results [30]. The lower limit of integral reflects the effects of superconductivity. The thermoelectric coefficient of an s-wave superconductor is exponentially smaller than  $\alpha_N$  at low temperatures  $\alpha \propto \alpha_N \exp(-\Delta/T) \ll \alpha_N$ .

- |   |   |
|---|---|
| <p>[1] G. Volovik, Zeroes in the energy gap in superconductors with high transition temperature, <i>Physics Letters A</i> <b>142</b>, 282 (1989).</p> <p>[2] K. Yang and S. L. Sondhi, Response of a <math>d_{x^2-y^2}</math> superconductor to a Zeeman magnetic field, <i>Phys. Rev. B</i> <b>57</b>, 8566 (1998).</p> <p>[3] D. F. Agterberg, P. M. R. Brydon, and C. Timm, Bogoliubov Fermi Surfaces in Superconductors with Broken Time-Reversal Symmetry, <i>Phys. Rev. Lett.</i> <b>118</b>, 127001 (2017).</p> <p>[4] P. M. R. Brydon, D. F. Agterberg, H. Menke, and C. Timm, Bogoliubov Fermi surfaces: General theory, magnetic order, and topology, <i>Phys. Rev. B</i> <b>98</b>, 224509 (2018).</p> <p>[5] H. Menke, C. Timm, and P. M. R. Brydon, Bogoliubov Fermi surfaces stabilized by spin-orbit coupling, <i>Phys. Rev. B</i> <b>100</b>, 224505 (2019).</p> <p>[6] C. Setty, Y. Cao, A. Kreisel, S. Bhattacharyya, and P. J. Hirschfeld, Bogoliubov Fermi surfaces in spin-<math>\frac{1}{2}</math> systems: Model Hamiltonians and experimental consequences, <i>Phys. Rev. B</i> <b>102</b>, 064504 (2020).</p> <p>[7] N. F. Q. Yuan and L. Fu, Zeeman-induced gapless superconductivity with a partial Fermi surface, <i>Phys. Rev. B</i> <b>97</b>, 115139 (2018).</p> <p>[8] R. Ohashi, S. Kobayashi, S. Kanazawa, Y. Tanaka, and</p> | <p>Y. Kawaguchi, Surface density of states and tunneling spectroscopy of a spin-<math>\frac{3}{2}</math> superconductor with Bogoliubov Fermi surfaces, <i>Phys. Rev. B</i> <b>110</b>, 104515 (2024).</p> <p>[9] C. Timm, A. P. Schnyder, D. F. Agterberg, and P. M. R. Brydon, Inflated nodes and surface states in superconducting half-Heusler compounds, <i>Phys. Rev. B</i> <b>96</b>, 094526 (2017).</p> <p>[10] C. Timm and A. Bhattacharya, Symmetry, nodal structure, and Bogoliubov Fermi surfaces for nonlocal pairing, <i>Phys. Rev. B</i> <b>104</b>, 094529 (2021).</p> <p>[11] T. Bzdušek and M. Sigrist, Robust doubly charged nodal lines and nodal surfaces in centrosymmetric systems, <i>Phys. Rev. B</i> <b>96</b>, 155105 (2017).</p> <p>[12] J. M. Link and I. F. Herbut, Bogoliubov-Fermi Surfaces in Noncentrosymmetric Multicomponent Superconductors, <i>Phys. Rev. Lett.</i> <b>125</b>, 237004 (2020).</p> <p>[13] S. Kobayashi, A. Bhattacharya, C. Timm, and P. M. R. Brydon, Bogoliubov Fermi surfaces from pairing of emergent <math>j = \frac{3}{2}</math> fermions on the pyrochlore lattice, <i>Phys. Rev. B</i> <b>105</b>, 134507 (2022).</p> <p>[14] C. Setty, S. Bhattacharyya, Y. Cao, A. Kreisel, and P. Hirschfeld, Topological ultranodal pair states in iron-based superconductors, <i>Nature communications</i> <b>11</b>, 523 (2020).</p> <p>[15] C. J. Lapp, G. Börner, and C. Timm, Experi-</p> |
|---|---|



- mental consequences of Bogoliubov Fermi surfaces, Phys. Rev. B **101**, 024505 (2020).
- [16] Z. Zhu, M. Papaj, X.-A. Nie, H.-K. Xu, Y.-S. Gu, X. Yang, D. Guan, S. Wang, Y. Li, C. Liu, J. Luo, Z.-A. Xu, H. Zheng, L. Fu, and J.-F. Jia, Discovery of segmented Fermi surface induced by Cooper pair momentum, Science **374**, 1381 (2021).
- [17] S. Banerjee, S. Ikegaya, and A. P. Schnyder, Anomalous Fano factor as a signature of Bogoliubov Fermi surfaces, Phys. Rev. Res. **4**, L042049 (2022).
- [18] Y. Mizukami, M. Haze, O. Tanaka, K. Matsuura, D. Sano, J. Böker, I. Eremin, S. Kasahara, Y. Matsuda, and T. Shibauchi, Unusual crossover from Bardeen-Cooper-Schrieffer to Bose-Einstein-condensate superconductivity in iron chalcogenides, Communications Physics **6**, 183 (2023).
- [19] T. Nagashima, K. Ishihara, K. Imamura, M. Kobayashi, M. Roppongi, K. Matsuura, Y. Mizukami, R. Grasset, M. Konczykowski, K. Hashimoto, and T. Shibauchi, Lifting of Gap Nodes by Disorder in Tetragonal FeSe<sub>1-x</sub>S<sub>x</sub> Superconductors, Phys. Rev. Lett. **133**, 156506 (2024).
- [20] Z. Yu, K. Nakamura, K. Inomata, X. Shen, T. Mikuri, K. Matsuura, Y. Mizukami, S. Kasahara, Y. Matsuda, T. Shibauchi, et al., Spin fluctuations from Bogoliubov Fermi surfaces in the superconducting state of S-substituted FeSe, Communications Physics **6**, 175 (2023).
- [21] Y. Sato, S. Kasahara, T. Taniguchi, X. Xing, Y. Kasahara, Y. Tokiwa, Y. Yamakawa, H. Kontani, T. Shibauchi, and Y. Matsuda, Abrupt change of the superconducting gap structure at the nematic critical point in FeSe<sub>1-x</sub>S<sub>x</sub>, Proceedings of the National Academy of Sciences **115**, 1227 (2018).
- [22] T. Hanaguri, K. Iwaya, Y. Kohsaka, T. Machida, T. Watashige, S. Kasahara, T. Shibauchi, and Y. Matsuda, Two distinct superconducting pairing states divided by the nematic end point in FeSe<sub>1-x</sub>S<sub>x</sub>, Science Advances **4**, eaar6419 (2018).
- [23] T. Nagashima, T. Hashimoto, S. Najafzadeh, S.-i. Ouchi, T. Suzuki, A. Fukushima, S. Kasahara, K. Matsuura, M. Qiu, Y. Mizukami, K. Hashimoto, Y. Matsuda, T. Shibauchi, S. Shin, and K. Okazaki, Discovery of nematic bogoliubov fermi surface in an iron-chalcogenide superconductor, Research Square 10.21203/rs.3.rs-2224728/v1 (2022).
- [24] A. Bhattacharya and C. Timm, Stability of bogoliubov fermi surfaces within bcs theory, Phys. Rev. B **107**, L220501 (2023).
- [25] D. Kim, S. Kobayashi, and Y. Asano, Quasiparticle on Bogoliubov Fermi Surface and Odd-Frequency Cooper Pair, Journal of the Physical Society of Japan **90**, 104708 (2021).
- [26] Y. Asano and A. Sasaki, Odd-frequency Cooper pairs in two-band superconductors and their magnetic response, Phys. Rev. B **92**, 224508 (2015).
- [27] T. Sato, S. Kobayashi, and Y. Asano, Discontinuous transition to a superconducting phase, Phys. Rev. B **110**, 144503 (2024).
- [28] T. Miki, S.-T. Tamura, S. Iimura, and S. Hoshino, Odd-frequency pairing inherent in a Bogoliubov Fermi liquid, Phys. Rev. B **104**, 094518 (2021).
- [29] Y. M. Gal'perin, V. Gurevich, and V. Kozub, Nonlinear acoustic effects in superconductors, Sov. Phys. JETP **65**, 1045 (1973).
- [30] Y. M. Galperin, V. Gurevich, and V. Kozub, Thermoelectric effects in superconductors, Sov. Phys. JETP **39**, 680 (1974).
- [31] M. J. Graf, S.-K. Yip, J. A. Sauls, and D. Rainer, Electronic thermal conductivity and the Wiedemann-Franz law for unconventional superconductors, Phys. Rev. B **53**, 15147 (1996).
- [32] P. Bureset, B. Lu, G. Tkachov, Y. Tanaka, E. M. Hankiewicz, and B. Trauzettel, Superconducting proximity effect in three-dimensional topological insulators in the presence of a magnetic field, Phys. Rev. B **92**, 205424 (2015).
- [33] B. S. Chandrasekhar, A NOTE ON THE MAXIMUM CRITICAL FIELD OF HIGH-FIELD SUPERCONDUCTORS, Applied Physics Letters **1**, 7 (1962).
- [34] A. M. Clogston, Upper Limit for the Critical Field in Hard Superconductors, Phys. Rev. Lett. **9**, 266 (1962).
- [35] J. Shabani, M. Kjaergaard, H. J. Suominen, Y. Kim, F. Nichele, K. Pakrouski, T. Stankevic, R. M. Lutchyn, P. Krogstrup, R. Feidenhans'l, S. Kraemer, C. Nayak, M. Troyer, C. M. Marcus, and C. J. Palmstrøm, Two-dimensional epitaxial superconductor-semiconductor heterostructures: A platform for topological superconducting networks, Phys. Rev. B **93**, 155402 (2016).
- [36] M. Kjaergaard, F. Nichele, H. Suominen, M. Nowak, M. Wimmer, A. Akhmerov, J. Folk, K. Flensberg, J. Shabani, w. C. Palmstrøm, et al., Quantized conductance doubling and hard gap in a two-dimensional semiconductor-superconductor heterostructure, Nature communications **7**, 12841 (2016).
- [37] C. M. Moehle, C. T. Ke, Q. Wang, C. Thomas, D. Xiao, S. Karwal, M. Lodari, V. van de Kerkhof, R. Termaat, G. C. Gardner, et al., InSbAs two-dimensional electron gases as a platform for topological superconductivity, Nano Letters **21**, 9990 (2021).
- [38] D. Phan, J. Senior, A. Ghazaryan, M. Hatefipour, W. M. Strickland, J. Shabani, M. Serbyn, and A. P. Higginbotham, Detecting Induced  $p \pm ip$  Pairing at the Al-InAs Interface with a Quantum Microwave Circuit, Phys. Rev. Lett. **128**, 107701 (2022).
- [39] C. Reeg, D. Loss, and J. Klinovaja, Metallization of a Rashba wire by a superconducting layer in the strong-proximity regime, Phys. Rev. B **97**, 165425 (2018).